Available online at www.sciencedirect.com
SCIENCE DIRECT®
PERGAMON
International Journal of Heat and Mass Transfer 46 (2003) 2571–2585
International Journal of HEAT and MASS TRANSFER
www.elsevier.com/locate/ijhmt

Modeling of plate heat exchangers with generalized configurations

Jorge A.W. Gut, José M. Pinto *

Department of Chemical Engineering, University of São Paulo, Av. Prof. Luciano Gualberto, trav. 3, 380, São Paulo, SP 05508-900, Brazil

Received 4 March 2002; received in revised form 9 January 2003

Abstract

A mathematical model is developed in algorithmic form for the steady-state simulation of gasketed plate heat exchangers with generalized configurations. The configuration is defined by the number of channels, number of passes at each side, fluid locations, feed connection locations and type of channel-flow. The main purposes of this model are to study the configuration influence on the exchanger performance and to further develop a method for configuration optimization. The main simulation results are: temperature profiles in all channels, thermal effectiveness, distribution of the overall heat transfer coefficient and pressure drops. Moreover, the assumption of constant overall heat transfer coefficient is analyzed.

Keywords: Plate heat exchanger; Mathematical modeling; Heat exchanger configuration

1. Introduction

For being compact, easy to clean, efficient and very flexible, the gasketed plate heat exchanger (PHE) is widely employed in the chemical, food and pharmaceutical process industries. The PHE consists of a pack of gasketed corrugated metal plates, pressed together in a frame (see Fig. 1). The gaskets on the corners of the plates form a series of parallel flow channels, where the fluids flow alternately and exchange heat through the thin metal plates. The number of plates, their perforation, the type and position of the gaskets and the location of the inlet and outlet connections at the covers characterize the PHE configuration, which further defines the flow distribution inside the plate pack. The flow distribution can be parallel, series or any of their various possible combinations.

The simplified thermal modeling of a PHE in steady state yields a linear system of first order ordinary differential equations, comprising the energy balance for each channel and the required boundary conditions. The main assumptions are as follows: plug-flow inside the channels, constant overall heat transfer coefficient throughout the exchanger, uniform distribution of flow in the channels, no heat loss and no heat exchange in the flow direction. This basic thermal model was presented by McKillop and Dunkley [1] and by Masubuchi and Ito [2] for some usual configurations. The Runge–Kutta–Gill integration method was used to solve the system of equations. The integration is non-trivial because the boundary conditions are defined in different extremes of the channel. Approximate solutions of the thermal model were developed by Settari and Venart [3] in polynomial form, and by Zaleski and Klepacka [4] in exponential form. Both methods lead to good approximations of the exact solution, but they may not be reliable when there is a large difference between fluid heat capacities.

Kandlikar and Shah [5] developed a method to calculate an approximate thermal effectiveness for large exchangers, where the effects of the end plates and of the

* Corresponding author. Present address: Department of Chemical and Biological Sciences and Engineering, Polytechnic University, Six Metrotech Center, Brooklyn, NY 11201, USA.
E-mail addresses: andrey@lscp.pqi.ep.usp.br (J.A.W. Gut), jpinto@poly.edu, jompinto@usp.br (J.M. Pinto).

0017-9310/03/$ - see front matter
doi:10.1016/S0017-9310(03)00040-1

Nomenclature

a	general model parameter
A	effective plate heat transfer area, m^2
b	channel average thickness, m
c	coefficient defined in Eqs. (A.3) and (A.4)
C_p	fluid specific heat at constant pressure, J/kg °C
d	parameter defined in Eq. (A.2b)
D_e	equivalent diameter of channel, m
D_P	port diameter of plate, m
E	exchanger thermal effectiveness, %
f	Fanning friction factor
g	gravitational acceleration, $g = 9.8$ m/s^2
G_C	channel mass velocity, kg/m^2 s
G_P	port mass velocity, kg/m^2 s
h	convective heat transfer coefficient, W/m^2 °C
k	fluid thermal conductivity, W/m °C
k_P	plate thermal conductivity, W/m °C
K	consistency parameter, Pa s^n
L	effective plate length for heat exchange, m
$\underline{\underline{M}}$	tridiagonal matrix defined in Eq. (A.2a)
n	flow index
N	number of channels per pass
N_C	number of channels
Nu	Nusselt number, $Nu = hD_e/k$
P	number of passes
Pr	Prandtl number, $Pr = C_p\mu/k$
R	fluid fouling factor, m^2 °C/W
Re	Reynolds number, $Re = G_C D_e/\mu$
s_i	channel i flow direction parameter, $s_i = +1$ or -1
T	temperature, °C
U	overall heat transfer coefficient, W/m^2 °C
w	effective plate width for heat exchange, m
W	fluid mass flow rate, kg/s
x	coordinate tangential to channel fluid flow, m
Y_f	binary parameter for type of channel-flow
Y_h	binary parameter for hot fluid location
$\underline{Z}$	eigenvector

Greek symbols

α	dimensionless heat transfer parameter defined in Eqs. (8a) and (8b)
β	chevron corrugation inclination angle, degrees
γ	shear rate, s^{-1}
ΔP	fluid pressure drop, Pa
ε_P	thickness of metal plate, m
η	dimensionless coordinate tangential to channel fluid flow
θ	dimensionless fluid temperature
$\underline{\theta}$	vector of channel dimensionless fluid temperatures
λ	eigenvalue
μ	fluid viscosity, Pa s
μ_g	generalized fluid viscosity for power law model, Pa s
ξ	duct geometrical parameter
ρ	fluid density, kg/m^3
υ	duct geometrical parameter
ϕ	parameter for feed connection relative location
Φ	plate area enlargement factor

Subscripts

c	cold fluid
h	hot fluid
i	ith element
in	fluid inlet
m	average
out	fluid outlet

Superscripts

I	side I of exchanger
II	side II of exchanger
side(i)	side that contains the ith channel, side(i) = I or II

changes of passes are less significant and therefore can be neglected. In this case, the exchanger is divided into a group of interconnected simpler exchangers with known effectiveness.

The analytical solution of the system of equations in matrix form was studied by Zaleski and Jarzebski [6] and Zaleski [7] for exchangers with series and parallel flow arrangements (see examples in Fig. 1). Since this solution method may lead to numerical problems on the calculation of eigenvalues and eigenvectors, it is not recommended to exchangers with large number of channels (see Appendix A).

Kandlikar and Shah [8] and Georgiadis and Macchietto [9] used the finite difference method for the simulation of PHEs. Kandlikar and Shah [8] simulated and compared several configurations. It was verified that higher effectiveness is achieved when the exchanger is symmetrical (both streams with the same number of passes) with the passes arranged for countercurrent flow in the channels. The same results were obtained by Zaleski and Klepacka [10] when analyzing the thermal effectiveness of various PHE configurations.

Asymmetrical configurations may yield adjacent channels with parallel flow and therefore a lower ther-

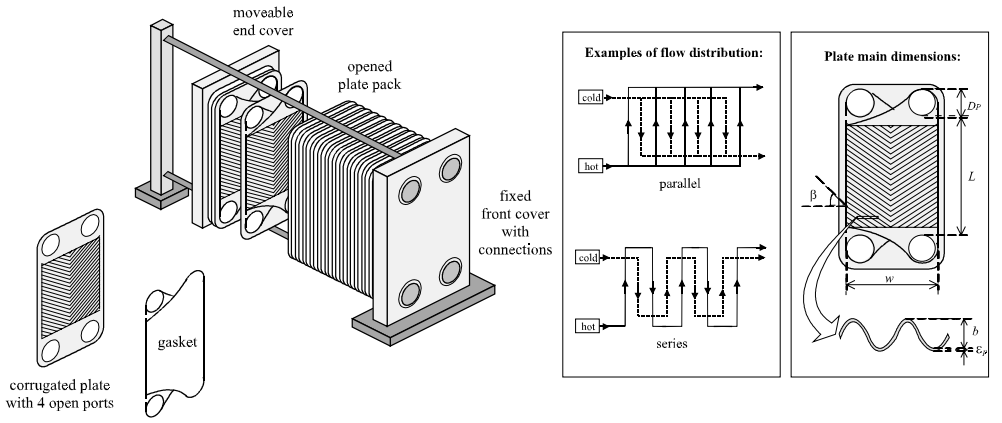

Fig. 1. The plate heat exchanger assemblage, examples of flow distributions and plate main dimensions.

mal effectiveness for the exchanger is achieved. However, when the fluids have very different flow rates or heat capacities, an asymmetrical configuration should be used depending on the allowable pressure drops. In such cases, there is no rigorous design method to select the best configuration, which is made by comparison among the most common pass-arrangements from thermal effectiveness and pressure drop viewpoints.

Georgiadis and Macchietto [9] presented a detailed modeling of a PHE used for milk pasteurization that couples the dynamic thermal model with the protein-fouling model. Three different configurations were compared and the reduction of the overall heat transfer coefficient, caused by the protein adhesion on the plates, was studied. The model was solved with the finite difference method, implemented in the software gPROMS [11].

To the authors knowledge there are no rigorous design methods for PHEs in the open literature, as there are for the shell-and-tube exchangers [12]. The design methods are mostly owned by the equipment manufacturers and are suited only for the marketed exchangers [13]. As an exception, Shah and Focke [14] have presented a detailed step-by-step design procedure for rating and sizing a PHE, which is, however, restricted to parallel flow arrangements.

In all of the aforementioned works, the overall heat transfer coefficient was considered invariable throughout the exchanger. For the thermal model, this assumption results in systems of linear differential equations, simplifying largely its mathematical solution. Nevertheless, there may be a considerable variation of the overall coefficient for some cases, such as the series flow arrangement with equal flow rates of the fluids [15].

The aim of this work is to present a PHE modeling framework that is suitable for any configuration. The purpose of developing such model is to study the influence of the configuration on the exchanger performance and to further develop an optimization method for rigorous configuration selection [16]. The variation of the overall heat transfer coefficient throughout the exchanger is also studied in this work, with respect to the assumption of a constant value.

The structure of this paper is as follows: first, the parameterization of the different configurations and the concept of equivalent configurations are presented, according to the work of Pignotti and Tamborenea [17]. Further, the mathematical modeling of a PHE is developed leading to its simplified and rigorous forms. Since it is not possible to generate a model that is explicitly a function of the configuration parameters, the mathematical modeling is developed in algorithmic form. Finally a simulation example is shown, where the effect of the assumption of constant overall heat transfer coefficient is analyzed.

2. Configuration characterization

The configuration of a PHE is defined by the information that allows the detailing of the equipment assemblage, including the connections on the fixed and moveable covers, the closed and open ports at each plate and the type and position of each gasket. To characterize such configuration, six distinct parameters are used: N_C, P^I, P^{II}, ϕ, Y_h and Y_f. These parameters are described as follows.

2.1. N_C: number of channels

A channel is the space comprised between two plates. The PHE can be represented by a row of channels numbered from 1 to N_C (see Fig. 2a). The odd-numbered channels belong to side I, and the even-numbered ones belong to side II (as an analogy to the "tube" and "shell" sides in a shell-and-tube exchanger). N_C^I and N_C^{II} denote the numbers of channels in each side. If N_C is

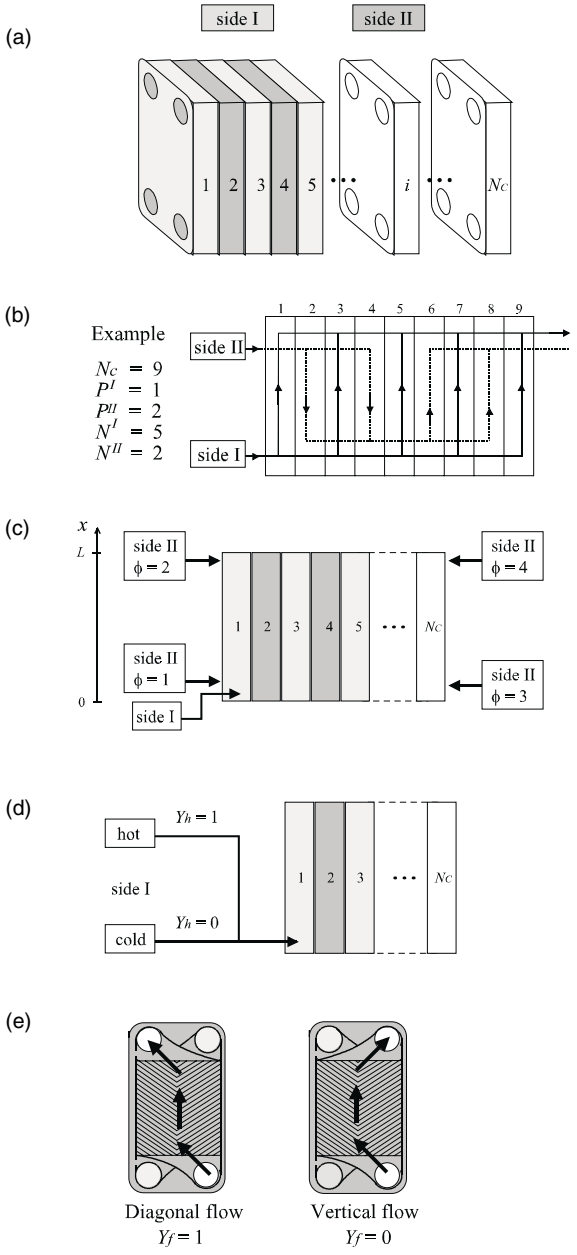

Fig. 2. Spatial characterization of the configuration parameters: (a) N_C; (b) example for P^I and P^{II}; (c) ϕ; (d) Y_h and (e) Y_f.

even, both sides have the same number of channels, otherwise side I has one more channel. Allowable values for $N_C : 2, 3, 4, 5, \ldots$

2.2. P^I and P^{II}: number of passes at sides I and II

A pass is a set of channels where the stream is split and distributed. For a regular configuration, each side of the PHE is divided into passes with the same number of channels per pass (N^I and N^{II}). Passes with different numbers of channels are unusual [13]. The relationship among N_C, P^I and P^{II} is given in Table 1 and an example is shown on Fig. 2b. Allowable values for P^I and P^{II}: respectively, the integer factors of N_C^I and N_C^{II}.

2.3. ϕ: feed connection relative location

The feed connection of side I is arbitrarily set to channel 1 at $x = 0$. The relative position of the feed of side II is given by the parameter ϕ, as shown in Fig. 2c [10,17]. The plate length x is not associated with the top and bottom of the PHE, neither channel 1 is associated with the fixed cover. The configuration can be freely rotated or mirrored to fit the PHE frame. Allowable values for ϕ: 1, 2, 3, and 4.

2.4. Y_h: hot fluid location

This binary parameter assigns the fluids to the exchanger sides (see Fig. 2d). If $Y_h = 1$, the hot fluid is at side I, and cold fluid is at side II. If $Y_h = 0$, the cold fluid is at side I, and hot fluid is at side II.

2.5. Y_f: type of flow in channels

Y_f is a binary parameter that defines the type of flow inside the channels. As shown in Fig. 2e, the flow can be vertical or diagonal, depending on the gasket type. The diagonal flow avoids the formation of stagnation areas, but the vertical flow type is easier to assemble. It is not possible to use both types together. If $Y_f = 1$, the flow is diagonal in all channels. If $Y_f = 0$, the flow is vertical in all channels.

The six parameters can represent any regular configuration, whose number of channels per pass is con-

Table 1
Relationship among numbers of channels and passes

Main equations			
$N_C = N_C^I + N_C^{II}$	$N_C^I = N^I P^I$	$N_C^{II} = N^{II} P^{II}$	
If N_C is *even*		If N_C is *odd*	
$N_C^I = \frac{N_C}{2}$	$N^I = \frac{N_C}{2P^I}$	$N_C^I = \frac{N_C+1}{2}$	$N^I = \frac{N_C+1}{2P^I}$
$N_C^{II} = \frac{N_C}{2}$	$N^{II} = \frac{N_C}{2P^{II}}$	$N_C^{II} = \frac{N_C-1}{2}$	$N^{II} = \frac{N_C-1}{2P^{II}}$

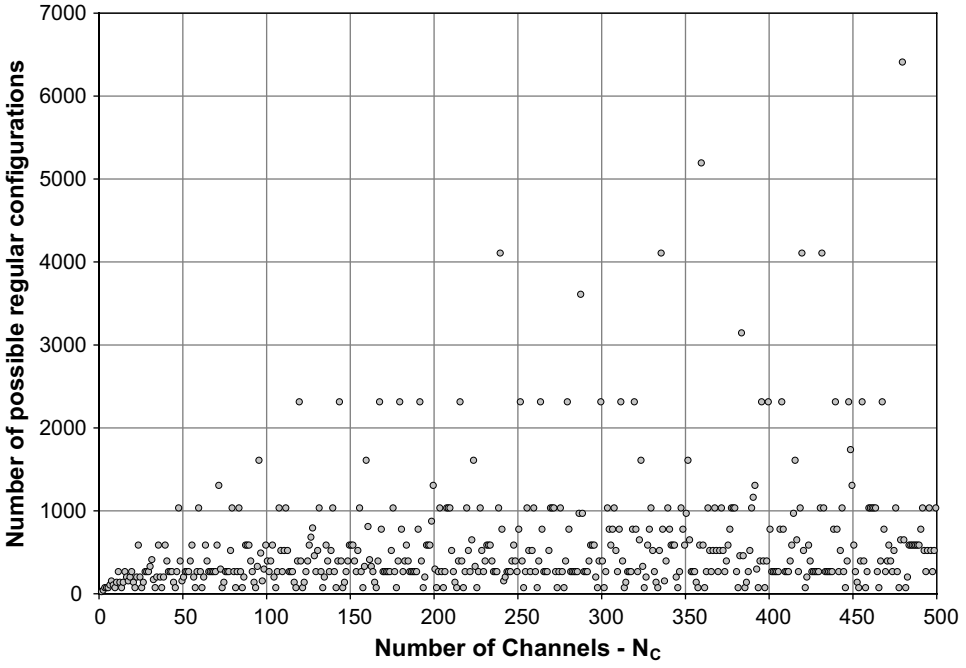

Fig. 3. Number of possible regular configurations as a function of the number of channels.

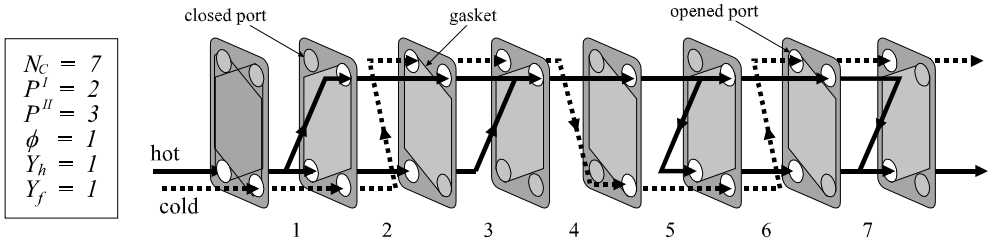

Fig. 4. Example of configuration for a PHE with eight plates.

stant at each side of the PHE [17]. A given number of channels, N_C, defines the set of allowable values of the five remaining parameters. The combination yields a finite number of possible regular configurations for each number of channels, as shown in Fig. 3. The disperse pattern is due to the variation of the number of integer factors of N_C^I and N_C^{II}, for each value of N_C.

A configuration example is illustrated in Fig. 4. It represents a PHE with eight plates (seven channels), where the hot fluid in side I ($Y_h = 1$) makes two passes ($P^I = 2$) and the cold fluid in side II makes three passes ($P^{II} = 3$). In this example, the inlet of side II is located next to the inlet of side I ($\phi = 1$, as in Fig. 2c) and the type of flow in the channels is diagonal ($Y_f = 1$). The parameter Y_f is mostly useful for the exchanger physical construction, but it may not be necessary for the simulation since its influence over the convective coefficients and friction factor is usually unknown.

3. Equivalent configurations

For a given value of number of channels and a fixed type of flow, there may exist equivalent configurations in terms of the thermal effectiveness and pressure drops. The identification of equivalent configurations is important to avoid redundant simulations. The equivalence relies on three remarks, as follows.

(A1) According to the property of flow reversibility, the inversion of the fluid flow direction in both sides does not alter the effectiveness of the PHE [17], nor the pressure drops if an elevation increase of length $(L + D_P)$ is always accounted for. This property is valid for the ideal case of no phase change, no heat losses and temperature-independent physical properties for the fluids [18].

(A2) When there is a single pass at one side, the flow direction is the same in all of its channels, regardless of the stream inlet and outlet locations at the first or last channels. A uniform distribution of flow throughout the channels is assumed here.

(A3) Simply inverting the direction of x, or numbering the channels in reverse order, may yield a new set of configuration parameters.

A methodology to detect equivalent configurations is presented in Table 2. For each set of N_C, P^I, P^{II} and Y_f, there are groups of values of the parameter ϕ that result in equivalent configurations. In the case of an even-numbered N_C, sides I and II have the same number of channels and can support the same passes. Therefore fluids can switch sides, which enables the equivalency between $Y_h = 0$ and $Y_h = 1$. For example, if $N_C = 20$, $P^I = 2$ and $P^{II} = 5$ (for any given value for Y_f), using $\phi = 1$ and $Y_h = 1$ is equivalent of using $\phi = 2$ and $Y_h = 0$ with $P^I = 5$ and $P^{II} = 2$ (see Table 2). An example of equivalency among four different configurations, their relationship and how remarks A1, A2 and A3 apply is shown in Fig. 5.

It is important to note that the single-pass "U-Type" exchanger, where the inlet and outlet connections are located at the fixed cover, cannot be represented directly by the proposed configuration parameters. However, due to remark A2, the "U-Type" exchanger is equivalent

Table 2
Identification of equivalent configurations

N_C	(P^I, P^{II})	Groups of equivalent values of ϕ
Odd[a]	(1, 1); (1, odd); (odd, 1)	{1, 3}; {2, 4}
	(1, even); (even, 1)	{1, 2, 3, 4}
	(odd, odd); (even, even)	{1}; {2}; {3}; {4}
	(odd, even); (even, odd)	{1, 2}; {3, 4}
Even[b]	(1, 1); (1, odd); (odd, 1)	{1h, 3h, 1c, 3c}; {2h, 4h, 2c, 4c}
	(1, even)h	{1h, 4h, 2c, 4c}; {2h, 3h, 1c, 3c}
	(even, 1)h	{1h, 3h, 2c, 3c}; {2h, 4h, 1c, 4c}
	(1, even)c	{1c, 4c, 2h, 4h}; {2c, 3c, 1h, 3h}
	(even, 1)c	{1c, 3c, 2h, 3h}; {2c, 4c, 1h, 4h}
	(odd, odd); (even, even)	{1h, 1c}; {2h, 2c}; {3h, 3c}; {4h, 4c}
	(odd, even); (even, odd)	{1h, 2c}; {2h, 1c}; {3h, 3c}; {4h, 4c}

[a] Equivalent configurations have the same value for Y_h (0 or 1).
[b] "h" denotes $Y_h = 1$ and "c" denotes $Y_h = 0$. When changing Y_h, switch P^I and P^{II}.

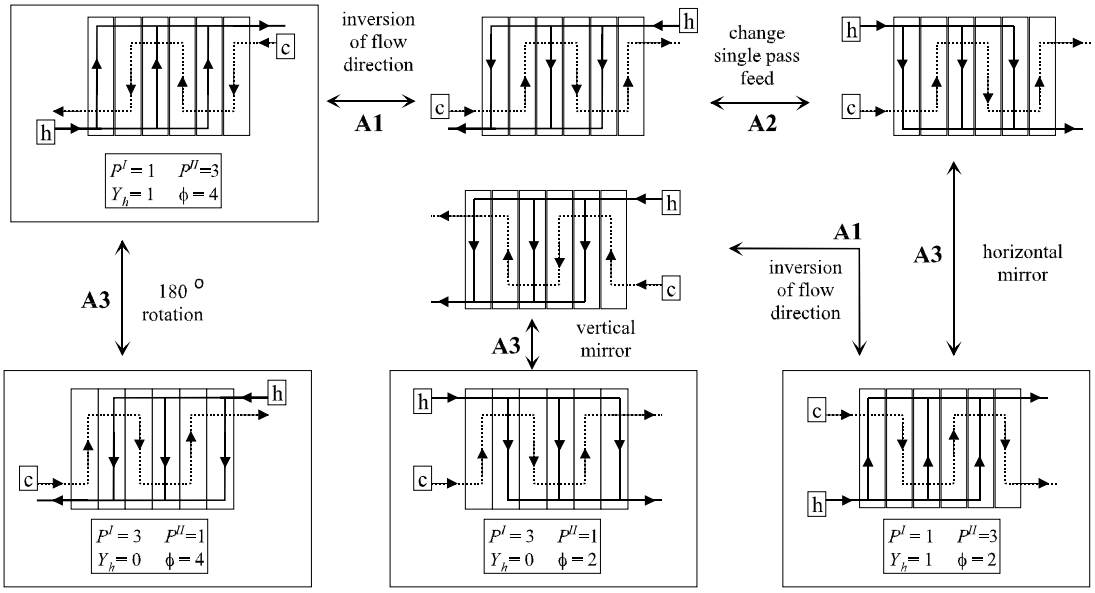

Fig. 5. Example of four equivalent configurations with $N_C = 6$ and $Y_f = 1$.

to a "Z-Type" exchanger, where inlet and outlet connections are located at opposite covers, which can be represented by the proposed parameters. Nevertheless, the assumption of equivalency between "U-Type" and "Z-Type" PHEs may not hold for exchangers with large number of channels because there may be a considerable difference in the flow and pressure distributions [19].

4. Mathematical modeling of the PHE

The following assumptions were considered in order to derive the mathematical model.

(B1) Steady-state operation.
(B2) No heat loss to the surroundings.
(B3) No heat exchange in the direction of flow.
(B4) Plug-flow inside the channels.
(B5) Uniform distribution of flow through the channels of a pass.
(B6) Perfect mixture of fluid in the end of a pass.
(B7) No phase changes.

The fluid inside a channel exchanges heat with the neighbor channels through the thin metal plates, as shown in Fig. 6 [1]. Applying the energy balance to the control volume shown in Fig. 6 it is possible to derive the differential equation for the channel temperature T_i, presented in Eq. (1), where Φ is the area enlargement factor (which accounts for the corrugation wrinkles) and U_i is the overall heat transfer coefficient between channels i and $i+1$.

$$\frac{\mathrm{d}T_i}{\mathrm{d}x} = \frac{s_i w \Phi U_{i-1}}{W_i C_{\mathrm{p}_i}}(T_{i-1} - T_i) + \frac{s_i w \Phi U_i}{W_i C_{\mathrm{p}_i}}(T_{i+1} - T_i) \tag{1}$$

The direction of flow in channel i is given by the binary variable s_i. If the flow follows the direction of x, then $s_i = +1$; otherwise, $s_i = -1$. The mass flow rate inside channel i, W_i, is obtained by Eq. (2) according to assumption B5. It is known that this assumption may not hold for passes with a large number of channels [19]. However, there is no rigorous modeling of this behavior. In Eq. (2), W_i depends on fluid-selection and on the number of channels per pass N (see Table 1), where side(i) refers to the side that contains channel i. The flow rates in each side, W^{I} and W^{II}, are associated to the hot and cold fluid flow rates through the parameter Y_{h} (see Fig. 2d).

$$W_i = \frac{W^{\mathrm{side}(i)}}{N^{\mathrm{side}(i)}}, \quad i = 1, \ldots, N_{\mathrm{C}}, \quad \mathrm{side}(i) = \{\mathrm{I}, \mathrm{II}\} \tag{2}$$

The overall heat transfer coefficient U_i between channels i and $i+1$ is given by Eq. (3) as a function of the fluid convective heat transfer coefficient h, the plate thermal conductivity k_{P}, the thickness of the plate ε_{P} and the fouling factors R_{h} and R_{c} for hot and cold streams, respectively (see Fig. 6 for a graphical representation of Eq. (3)).

$$\frac{1}{U_i} = \frac{1}{h_i} + \frac{1}{h_{i+1}} + \frac{\varepsilon_{\mathrm{P}}}{k_{\mathrm{P}}} + R_{\mathrm{h}} + R_{\mathrm{c}}, \quad i = 1, \ldots, (N_{\mathrm{C}} - 1) \tag{3}$$

The length of the path x and the channel fluid temperature $T_i(x)$ are converted into dimensionless form

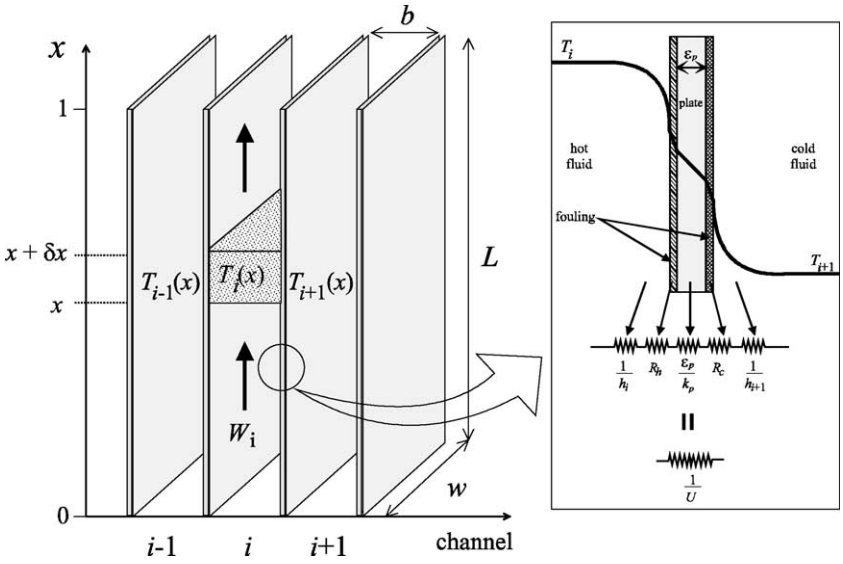

Fig. 6. Control volume for derivation of energy balance in an upward flow channel.

Table 3
Thermal boundary conditions for the PHE modeling

Boundary condition	Equation form
Fluid inlet: the temperature at the entrance of the first pass is the same as the stream inlet temperature	$\theta_i(\eta) = \theta_{\text{fluid,in}}, \quad i \in \text{first pass}$
Change of pass: there is a perfect mixture of the fluid leaving the channels of a pass, before entering the next one	$\theta_i(\eta) = \frac{1}{N}\sum_{j\in\text{previous pass}}^{N}\theta_j(\eta), \quad i \in \text{current pass}$
Fluid outlet: the stream outlet temperature results from a perfect mixture of the fluid leaving the last pass	$\theta_{\text{fluid,out}} = \frac{1}{N}\sum_{j\in\text{last pass}}^{N}\theta_j(\eta)$

using Eqs. (4) and (5). The dimensionless differential equations for channel temperature are presented in Eqs. (6a)–(6c), where $A = \Phi wL$ is the effective plate heat exchange area.

$$\eta(x) = \frac{x}{L}, \quad 0 \leqslant \eta \leqslant 1 \tag{4}$$

$$\theta_i(T_i) = \frac{T_i - T_{\text{c,in}}}{T_{\text{h,in}} - T_{\text{c,in}}}, \quad 0 \leqslant \theta \leqslant 1 \tag{5}$$

$$\frac{\mathrm{d}\theta_1}{\mathrm{d}\eta} = \frac{s_1 A}{W_1 C_{\text{p}_1}}[U_1(\theta_2 - \theta_1)] \quad \text{first channel} \tag{6a}$$

$$\frac{\mathrm{d}\theta_i}{\mathrm{d}\eta} = \frac{s_i A}{W_i C_{\text{p}_i}}[U_{i-1}(\theta_{i-1} - \theta_i) + U_i(\theta_{i+1} - \theta_i)] \quad \text{channel } i\text{: } (1 < i < N_{\text{C}}) \tag{6b}$$

$$\frac{\mathrm{d}\theta_{N_{\text{C}}}}{\mathrm{d}\eta} = \frac{s_{N_{\text{C}}} A}{W_{N_{\text{C}}} C_{\text{p}_{N_{\text{C}}}}}[U_{N_{\text{C}}-1}(\theta_{N_{\text{C}}-1} - \theta_{N_{\text{C}}})] \quad \text{last channel} \tag{6c}$$

The overall heat transfer coefficient is a function of the fluid temperature in the channels (Eq. (3)), which depends on η. Since this makes U_i also a function of η, the solution of the system of differential Eqs. (6a)–(6c) is not straightforward. However, if the fluid physical properties are assumed constant, Eqs. (6) can be simplified to Eqs. (7), where the coefficients α^{I} and α^{II} are given, respectively, by Eqs. (8a) and (8b) as functions of the constant overall heat transfer coefficient U. Note that channel 1 is always assigned to side I (Eq. (7a)).

$$\frac{\mathrm{d}\theta_1}{\mathrm{d}\eta} = s_1\alpha^{\text{I}}(-\theta_1 + \theta_2) \quad \text{first channel} \tag{7a}$$

$$\frac{\mathrm{d}\theta_i}{\mathrm{d}\eta} = s_i\alpha^{\text{side}(i)}(\theta_{i-1} - 2\theta_i + \theta_{i+1}) \quad \text{channel } i\text{: } (1 < i < N_{\text{C}}),\ \text{side}(i) = \{\text{I}, \text{II}\} \tag{7b}$$

$$\frac{\mathrm{d}\theta_{N_{\text{C}}}}{\mathrm{d}\eta} = s_{N_{\text{C}}}\alpha^{\text{side}(N_{\text{C}})}(\theta_{N_{\text{C}}-1} - \theta_{N_{\text{C}}}) \quad \text{last channel},\ \text{side}(N_{\text{C}}) = \{\text{I}, \text{II}\} \tag{7c}$$

$$\alpha^{\text{I}} = \frac{AUN^{\text{I}}}{W^{\text{I}}C^{\text{I}}_{\text{p}_\text{m}}} \tag{8a}$$

$$\alpha^{\text{II}} = \frac{AUN^{\text{II}}}{W^{\text{II}}C^{\text{II}}_{\text{p}_\text{m}}} \tag{8b}$$

Consequently, the system of Eqs. (6a)–(6c) is reduced to a linear system of ordinary differential Eqs. (7a)–(7c), which can be solved analytically. For details on the analytical solution of such system, please refer to Appendix A.

The necessary thermal boundary conditions for both the simplified model (defined by Eqs. (7)) and the distributed-U model (defined by Eqs. (3) and (6)) are presented in Table 3. Every channel requires a boundary condition equation for its inlet temperature. The inlet position of channel i is determined by the value of s_i. If $s_i = +1$, the inlet is located at position $\eta = 0$; otherwise the inlet is located at $\eta = 1$. The number and structure of the required boundary equations must be defined according to the configuration parameters. For example, Eqs. (9a)–(9i) are the boundary conditions for the PHE in Fig. 4

$$\theta_1(\eta = 0) = \theta_{\text{h,in}} = 1 \tag{9a}$$

$$\theta_2(\eta = 0) = \theta_{\text{c,in}} = 0 \tag{9b}$$

$$\theta_3(\eta = 0) = \theta_{\text{h,in}} = 1 \tag{9c}$$

$$\theta_4(\eta = 1) = \theta_2(\eta = 1) \tag{9d}$$

$$\theta_5(\eta = 1) = \frac{\theta_1(\eta = 1) + \theta_3(\eta = 1)}{2} \tag{9e}$$

$$\theta_6(\eta = 0) = \theta_4(\eta = 0) \tag{9f}$$

$$\theta_7(\eta = 1) = \frac{\theta_1(\eta = 1) + \theta_3(\eta = 1)}{2} \tag{9g}$$

$$\theta_{\text{h,out}} = \frac{\theta_5(\eta = 0) + \theta_7(\eta = 0)}{2} \tag{9h}$$

$$\theta_{\text{c,out}} = \theta_6(\eta = 1) \tag{9i}$$

The thermal effectiveness and the pressure drop calculations are needed for performance evaluation of the heat exchanger. Once the system of equations is solved and the outlet temperatures are obtained, the exchanger thermal effectiveness E is calculated using Eq. (10a) (side I as reference) or (10b) (side II as reference). Note that

the overall energy conservation implies that $E = E^{I} = E^{II}$.

$$E^{I} = \frac{W^{I}C^{I}_{p_m}|\theta_{in} - \theta_{out}|^{I}}{\min(W^{I}C^{I}_{p_m}, W^{II}C^{II}_{p_m})} \tag{10a}$$

$$E^{II} = \frac{W^{II}C^{II}_{p_m}|\theta_{in} - \theta_{out}|^{II}}{\min(W^{I}C^{I}_{p_m}, W^{II}C^{II}_{p_m})} \tag{10b}$$

The dimensionless forms of Eqs. (10a) and (10b), presented in Eqs. (10c) and (10d), are obtained using Eqs. (8a) and (8b) and may be used with the simplified simulation model.

$$E^{I} = \frac{N^{I}}{\alpha^{I}} \max\left(\frac{\alpha^{I}}{N^{I}}, \frac{\alpha^{II}}{N^{II}}\right)|\theta_{in} - \theta_{out}|^{I} \tag{10c}$$

$$E^{II} = \frac{N^{II}}{\alpha^{II}} \max\left(\frac{\alpha^{I}}{N^{I}}, \frac{\alpha^{II}}{N^{II}}\right)|\theta_{in} - \theta_{out}|^{II} \tag{10d}$$

The fluid pressure drop at sides I and II, ΔP^{I} and ΔP^{II}, can be calculated by Eq. (11) [13,14]. The first term in the right-hand side evaluates the friction loss inside the channels, where G_C denotes the channel mass velocity (Eq. (12a)), f is the Fanning friction factor, D_e is the channel equivalent diameter (Eq. (13)) and the channel dimensions are shown in Fig. 1. The second term in the right-hand side represents the pressure drop for port flow, where G_P is the port mass velocity (Eq. (12b)). The last term is the pressure variation due to an elevation change. Since the gravitational acceleration direction is not necessarily associated to the vertical dimension η and there is no information on the pump location, this term is always considered. Therefore, the pressure drop may be overestimated.

$$\Delta P = \left(\frac{2f(L + D_P)PG_C^2}{\rho_m D_e}\right) + 1.4\left(P\frac{G_P^2}{2\rho_m}\right) + \rho_m g(L + D_P) \quad \text{for sides I and II} \tag{11}$$

$$G_C = \frac{W}{Nbw} \quad \text{for sides I and II} \tag{12a}$$

$$G_P = \frac{4W}{\pi D_P^2} \quad \text{for sides I and II} \tag{12b}$$

$$D_e = \frac{4bw}{2(b + w\Phi)} \approx \frac{2b}{\Phi} \tag{13}$$

The necessary correlations for the calculation of convective coefficients and friction factors are presented in Eqs. (14a) and (14b). Usual values for the empirical parameters a_1 to a_6 are supplied in the works of Shah and Focke [14], Saunders [20] and Mehrabian et al. [21].

$$Nu = a_1 Re^{a_2} Pr^{a_3} \quad \text{for sides I and II} \tag{14a}$$

$$f = a_4 + \frac{a_5}{Re^{a_6}} \quad \text{for sides I and II} \tag{14b}$$

If the fluid has non-Newtonian behavior, Re and Pr should be calculated using the generalized viscosity, μ_g, defined in Eq. (15a) for the reological model of power law (note that μ_g is not the apparent viscosity). The definition of the geometric parameters υ and ξ is presented by Delplace and Leuliet [22] for cylindrical ducts of arbitrary cross-section, including the PHE channel. Since the power law parameters n and K are valid for a certain range of shear rate, Eq. (15b) is important to evaluate the shear rate at the plate wall, γ, and thus validate the PHE simulation results.

$$\mu_g = K\xi^{n-1}\left(\frac{G_C}{\rho D_e}\right)^{n-1}\left(\frac{\upsilon n + 1}{(\upsilon + 1)n}\right)^{n} \tag{15a}$$

$$\gamma = \xi\left(\frac{G_C}{\rho D_e}\right)\left(\frac{\upsilon n + 1}{(\upsilon + 1)n}\right) \tag{15b}$$

In summary, the distributed-U mathematical thermal modeling of a PHE is defined by Eq. (3) (overall heat transfer coefficient), Eqs. (6a)–(6c) (channel fluid temperature), Eqs. (10a) and (10b) (thermal effectiveness), Eqs. in Table 3 (boundary conditions), Eq. (14a) and the equations for the temperature dependence of the physical properties of the fluids. For the simplified model, in which a constant overall heat transfer coefficient is assumed, the new channel fluid temperature equations are Eqs. (7a)–(7c) where the heat transfer parameters α^{I} and α^{II} are obtained with Eqs. (8a) and (8b). For the calculation of U, one must assume a certain thermal effectiveness for the PHE, calculate the corresponding outlet temperatures of the fluids and then the average values of their physical properties. The constant convective coefficients h_{hot} and h_{cold} are obtained with Eq. (14a) and they are used in Eq. (3) to evaluate U. For both distributed-U and simplified models the pressure drops are calculated with Eqs. (11) and (14b) using the average values for fluid physical properties.

5. Simulation of PHEs with generalized configurations

The mathematical modeling of a PHE, for the calculation of its thermal effectiveness and fluid pressure drops, was presented in the previous section. However, it is not possible to derive a model that is explicitly a function of the configuration parameters, especially because of the binary variable s_i and the required thermal boundary conditions shown in Table 3. To overcome this limitation, the mathematical modeling for generalized configurations was developed in the form of an "assembling algorithm". Given the configuration parameters, this algorithm guides the construction of the complete mathematical model of the PHE and the simulation at steady state operation. The assembling algorithm for the simplified model has 13 steps as follows.

(1) The required data for the PHE $(L, w, b, D_P, \varepsilon_P, \Phi, k_P)$, for the hot and cold fluids $(T_{in}, W, \rho_m, \mu_m, C_{p_m}, k_m, R, a_1, \ldots, a_6)_{hot,cold}$ and the configuration parameters $(N_C, P^I, P^{II}, \phi, Y_h, Y_f)$ are read.
(2) The parameter Y_h assigns all fluid data to sides I and II.
(3) The number of channels per pass at each side, N^I and N^{II}, are calculated depending on the value of N_C (see Table 1).
(4) Pressure drops for both sides of the PHE, ΔP^I and ΔP^{II}, are calculated with Eqs. (11), (12) and (14b).
(5) Coefficients α^I and α^{II} are obtained by Eqs. (8), using U, which is obtained from Eq. (3) using the constant convective heat transfer coefficients h^I and h^{II} (Eq. (14a)).
(6) The values of s_i $(i = 1, \ldots, N_C)$ are determined. These depend on the configuration parameters N_C, P^I, P^{II} and ϕ. The structure of this step is presented in Appendix B.
(7) The assembling of the system of equations starts with the differential equations for the PHE inner channels, using Eq. (7b).
(8) Differential equations for the temperature in the first and last channels (Eqs. (7a) and (7c), respectively) are included in the system.
(9) Boundary conditions for the channels in side I are generated in the format shown in Table 3. The fluid path inside the exchanger, from inlet to outlet, needs to be followed in order to determine the connections among the channels and passes. See Appendix B for the detailing of this step.
(10) Boundary conditions for side II are also generated. However, each value of the parameter ϕ requires a specific treatment. The parameters N_C and P^{II} determine the fluid path of side II, and ϕ determines the flow direction inside this path and thus the connections of the channels of each pass and the boundary conditions defined at $\eta = 0$ and $\eta = 1$. Details are presented in Appendix B.
(11) Equations of thermal effectiveness for both sides, E^I and E^{II}, are included in dimensionless form (Eqs. (10c) and (10d)).
(12) The resulting system of equations, defined by the differential equations on the temperature in each channel, the boundary conditions equations and the effectiveness equations, is solved by numerical or analytical methods.
(13) The main simulation results, such as pressure drops and outlet temperatures for sides I and II (which are assigned to the hot and cold streams using Y_h), as well as the PHE thermal effectiveness, are obtained.

The derivation of the assembling algorithm for the distributed-U model is straightforward. Since coefficients α^I and α^{II} are no longer used, step 5 should be discarded. Eqs. (6a)–(6c) need to be used instead of Eqs. (7a)–(7c) (which are in dimensionless form). The equations for the hot and cold fluids physical properties dependence upon temperature for each channel (C_{p_i}, μ_i and k_i, $1 \leqslant i \leqslant N_C$) are needed in the system of equations. Note that the even-numbered and odd-numbered channels contain different fluids (which are assigned to sides I and II by the configuration parameter Y_h) and therefore are described by different equations of physical properties.

The equations for the channel dimensionless numbers (Re_i, Nu_i and Pr_i, $1 \leqslant i \leqslant N_C$) and the correlation for their relationship (Eq. (14a)) need to be included in the system of equations. Finally, Eq. (3)) for overall heat transfer coefficients U_i $(1 \leqslant i \leqslant N_C - 1)$ are also required in the system of equations. In step 11, Eqs. (10a) and (10b) for the effectiveness calculation are to be used instead of Eqs. (10c) and (10d) (which depend on α^I and α^{II}).

In step 12, the solution of the simplified model can be carried out by both analytical (see Appendix A) or numerical methods. For the distributed-U model, the modifications increase largely the size and complexity of the generated system of equations (which is no longer linear), hence a numerical solution approach is necessary. In this work, a second order centered finite difference method was adopted in the implementation of the assembling algorithm for both simplified and distributed-U models. In the finite difference method, all variables depending on the plate length η are discretized with respect to this dimension. Several schemes were tested and 20 discretization intervals within $\eta = [0, 1]$ showed to be enough to obtain excellent numerical results. In the work of Georgiadis and Macchietto [9], a similar discretization scheme was used for the dynamic simulation of PHEs that yields accurate results.

The software gPROMS [11] is used for the problem solution. A computer program was developed to run steps 1–11 of the assembling algorithm. After reading the data, the program makes all necessary calculations, generates a report and creates the formatted input file for gPROMS. This procedure made the simulation of different configurations much simpler and flexible.

6. Simulation example

The assembling algorithm presented in the last section was applied for the simulation of the process of cooling a sucrose solution (60° Brix) using cold water in a PHE with 36 channels and a symmetrical configuration. Both simplified and distributed-U models were used and the results were compared. The required data for this problem is shown in Table 4. The inlet temperatures were selected to obtain a large variation on the viscosity of the sucrose solution that is a viscous Newtonian fluid. Eqs. (16) and (17), were used for the tem-

Table 4
Required data for the example of simulation

Plates (stainless steel 360, chevron)		Configuration	
$L = 74.0$ cm	$\beta = 45°$		
$w = 23.6$ cm	$\Phi = 1.17$	$N_C = 36$	$\phi = 3$
$b = 2.7$ mm	$\varepsilon_P = 0.7$ mm	$P^I = 2$	$Y_h = 1$
$D_P = 5.9$ cm	$k_P = 17$ W/m °C [20]	$P^{II} = 2$	$Y_f = 1$
Hot fluid (sucrose sol. 60° Brix)	**Cold fluid (clean water)**		
$T_{in,hot} = 35.0$ °C	$T_{in,cold} = 1.0$ °C		
$W_{hot} = 1.30$ kg/s	$W_{cold} = 1.30$ kg/s		
$R_{f,hot} = 8.6 \times 10^{-5}$ m² °C/W [23]	$R_{f,cold} = 1.7 \times 10^{-5}$ m² °C/W [23]		
$\rho_{hot} = 1286$ kg/m³ [24]	$\rho_{cold} = 1000$ kg/m³ [26]		
$\mu_{hot} = 5.15 \times 10^{-2}$ Pa s [24]	$\mu_{cold} = 1.33 \times 10^{-3}$ Pa s [27]		
$C_{Phot} = 2803$ J/kg °C [25]	$C_{Pcold} = 4206$ J/kg °C [28]		
$k_{hot} = 0.407$ W/m °C [24]	$k_{cold} = 0.584$ W/m °C [26]		
$a_{1,hot} = 0.400$ [20]	$a_{1,cold} = 0.300$ [20]		
$a_{2,hot} = 0.598$ [20]	$a_{2,cold} = 0.663$ [20]		
$a_{3,hot} = 0.333$ [20]	$a_{3,cold} = 0.333$ [20]		
$a_{4,hot} = 0.000$ [20]	$a_{4,cold} = 0.000$ [20]		
$a_{5,hot} = 18.29$ [20]	$a_{5,cold} = 1.441$ [20]		
$a_{6,hot} = 0.652$ [20]	$a_{6,cold} = 0.206$ [20]		

perature-dependence of the physical properties when using the distributed-U model. For the simplified model, the average properties were estimated assuming a thermal effectiveness of 75 % for the PHE (units as in the nomenclature)

$$\rho = -1.451 \times 10^{-3} T^2 - 0.4281 T + 1296 \quad (\text{sucrose } 60° \text{ Brix},\ 0 \leqslant T \leqslant 60\ °\text{C}) \quad [24] \tag{16a}$$

$$\log(\mu) = -4.513 + \frac{421.8}{T + 108.5} \quad (\text{sucrose } 60° \text{ Brix},\ 0 \leqslant T \leqslant 80\ °\text{C}) \quad [24] \tag{16b}$$

$$C_p = 4.803 T + 2696 \quad (\text{sucrose } 60° \text{ Brix},\ 0 \leqslant T \leqslant 100\ °\text{C}) \quad [25] \tag{16c}$$

$$k = -3.696 \times 10^{-6} T^2 + 1.201 \times 10^{-3} T + 0.3825 \quad (\text{sucrose } 60° \text{ Brix},\ 0 \leqslant T \leqslant 80\ °\text{C}) \quad [24] \tag{16d}$$

$$\rho = 2.080 \times 10^{-5} T^3 - 6.668 \times 10^{-3} T^2 + 0.04675 T + 999.9 \quad (\text{water},\ 0 \leqslant T \leqslant 90\ °\text{C}) \quad [26] \tag{17a}$$

$$\frac{1}{\mu} = 21.482 \left[(T - 8.435) + \sqrt{8078.4 + (T - 8.435)^2} \right] - 1200 \quad (\text{water},\ 0 \leqslant T \leqslant 100\ °\text{C}) \quad [27] \tag{17b}$$

$$C_p = 5.2013 \times 10^{-7} T^4 - 2.1528 \times 10^{-4} T^3 + 4.1758 \times 10^{-2} T^2 - 2.6171 T + 4227.1 \quad (\text{water},\ 0 \leqslant T \leqslant 260\ °\text{C}) \quad [28] \tag{17c}$$

$$k = 0.5692 + \frac{T}{538} - \frac{T^2}{133,333} \quad (\text{water},\ 0 \leqslant T \leqslant 90\ °\text{C}) \quad [26] \tag{17d}$$

The main simulation results are presented in Table 5 and the temperature profiles in the channels and distribution of the temperature difference between channels (obtained by the distributed-U model) are presented in Fig. 7a and b, respectively. The distribution of the overall heat transfer coefficient throughout the exchanger is shown in Fig. 7c for both mathematical models. The results from the distributed-U model show

Table 5
Main results for the simulation example

Variable	Distributed-U model	Simplified model	Deviation (%)
PHE thermal effectiveness (%)	73.4	73.9	0.7
Sucrose solution outlet temp. (°C)	10.0	9.9	1.0
Water outlet temp. (°C)	17.6	17.7	0.6
Sucrose solution pressure drop (kPa)	81.4		–
Water pressure drop (kPa)	21.1		–
Number of variables after discretization	6795	760	–
CPU time on 450 MHz PC (s)	8.6	0.3	–

that U varies from 866 to 1219 W/m^2 °C, whereas the simplified model was solved with an average value of 1046 W/m^2 °C. Despite this significant difference, the main simulation results obtained by both models are very close (see Table 5), with a deviation of only 0.7% for the exchanger effectiveness.

The difference between the temperature profiles obtained by both models is not significant. The largest deviation obtained is 0.82 °C for the profile of channel 17 around $\eta = 0.7$. The average absolute deviation for this problem is 0.48 °C. When processing thermal-sensitive products, the analysis of the temperature profiles (like the ones in Fig. 7a) is important to determine the maximum and minimum temperatures of the product in the PHE. It is interesting to note in Fig. 7b that at the bottom part of plate 19, the sucrose solution is being heated up. This occurs because plate 19 is located near the change of passes of sides I and II. As already noted by Kandlikar and Shah [5], the first and last channels and the ones adjacent to the changes of pass have a lower thermal efficiency. Bassiouny and Martin [29] have also pointed out that reversed or zero heat flow may be obtained in the central plates of a multi-pass PHE due to the iteration among passes.

The assembling algorithm allows the study of the sensitivity of the PHE performance to the configuration parameters. For instance, parameter ϕ does not affect the pressure drop calculation, however, it influences the thermal effectiveness of the PHE. For this simulation example, if $\phi = 1$ is used instead of $\phi = 3$ (see Fig. 2c), the flow between adjacent channels is mostly parallel and the effectiveness of the exchanger drops from 73.4% to 58.1%. This shows how critical the selection of the configuration of a PHE can be. The fully usage of the admissible pressure drops of hot and cold streams cannot assure the highest effectiveness if a poor configuration is selected.

Several simulation examples comprising different configurations, fluids and plate geometries were made. It was verified that even with a remarkable difference in the distribution of the overall heat transfer coefficient, there is a small difference between the main simulation results obtained from both distributed-U and simplified models. The obtained deviations between models were under 1.5%, with respect to E. It was also verified that remark A1 (for equivalent configurations) holds for the distributed-U model, i.e. the difference among the effectiveness of equivalent PHEs calculated by the distributed-U model is small.

The number of variables after the discretization by the finite difference method is approximately nine times larger for the distributed-U model. To make the solution of large exchangers achievable, the "block decomposition" option of gPROMS is used, where the system of equations is decomposed into smaller systems. Even with this option, the solution of exchangers with hundreds of plates using the distributed-U model requires 1–15 min in a 450 MHz PC with 128 Mb-RAM, depending on the exchanger configuration. For the case of smaller exchangers, as the example, the solution is achieved within seconds (see Table 5).

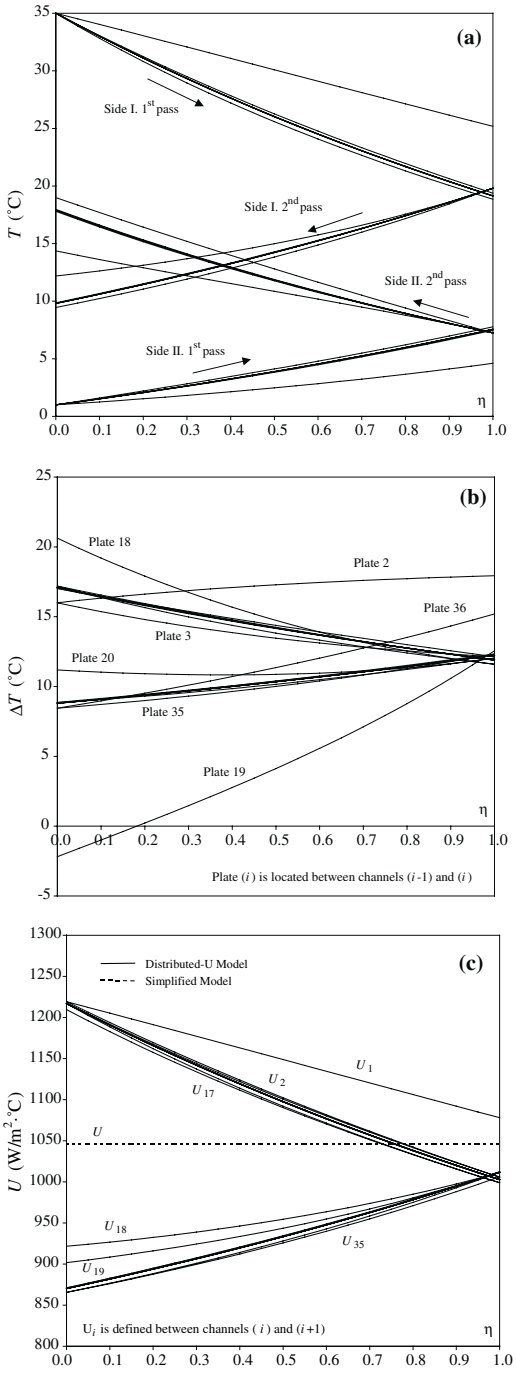

Fig. 7. Distribution of temperature and overall heat transfer coefficient throughout the PHE for the simulation example.

7. Conclusions

The configuration of a plate heat exchanger (PHE) was characterized by a set of six parameters and a methodology to detect equivalent configurations was presented. Based on this parameterization, a detailed mathematical model for the simulation of a PHE in steady-state with a general configuration was developed in algorithmic form. This assembling algorithm made the simulation and comparison of different configurations more flexible. An important feature of the proposed algorithm is that it may be coupled to any procedure to solve the system of differential and algebraic equations.

The assumption of constant overall heat transfer coefficient throughout the exchanger, often used for the mathematical modeling, was tested and showed little influence over the main simulation results for heat exchange (thermal effectiveness and outlet temperatures).

The presented assembling algorithm is an important tool for the study of the influence of the configuration on the exchanger performance, and can be further used to develop optimization methods for selecting the plate heat exchanger configuration. Research in this area is currently under development [16].

Acknowledgements

The authors would like to thank the financial support from FAPESP (grants 98/15808-1 and 00/13635-4).

Appendix A. Analytical solution of the PHE thermal model

The thermal modeling of a PHE, assuming constant fluid physical properties, yields a linear system of ordinary differential equations, previously presented in Eqs. (7a)–(7c). This system is represented in matrix form in Eq. (A.1) [7], where the structure of the tridiagonal matrix $\underline{\underline{M}}$ is shown is Eqs. (A.2a) and (A.2b) and $\underline{\theta}$ is the vector of channel dimensionless fluid temperatures $\theta_i(\eta)$

$$\frac{\mathrm{d}\underline{\theta}}{\mathrm{d}\eta} = \underline{\underline{M}}\underline{\theta} \tag{A.1}$$

$$\underline{\underline{M}} = \begin{bmatrix} -d_1 & +d_1 & 0 & 0 & \cdots & 0 \\ +d_2 & -2d_2 & +d_2 & 0 & \cdots & 0 \\ 0 & +d_3 & -2d_3 & +d_3 & & \vdots \\ \vdots & & & & & 0 \\ 0 & \cdots & 0 & +d_{N_C-1} & -2d_{N_C-1} & +d_{N_C-1} \\ 0 & \cdots & 0 & 0 & +d_{N_C} & -d_{N_C} \end{bmatrix} \tag{A.2a}$$

$$d_i = s_i \alpha^{\mathrm{side}(i)}, \quad i = 1, \ldots, N_C, \quad \mathrm{side}(i) = \{\mathrm{I}, \mathrm{II}\} \tag{A.2b}$$

The solution of Eq. (A.1) is given by Eq. (A.3), where λ_j and $\underline{Z_j}$ are, respectively, the corresponding eigenvalues and eigenvectors of matrix $\underline{\underline{M}}$ [30].

$$\underline{\theta}(\eta) = \sum_{j=1}^{N_C} c_j \underline{Z_j} \exp(\lambda_j \eta) \tag{A.3}$$

In order to determine the coefficients c_j, the "fluid inlet" and "change of pass" boundary conditions (see Table 3) must be applied to generate a linear system of algebraic equations whose variables are c_j ($1 \leqslant j \leqslant N_C$). The system can be solved by using techniques such as Gaussian elimination or LU matrix decomposition [30].

Zaleski and Jarzebski [6] showed that matrix $\underline{\underline{M}}$ has one null eigenvalue and that there may be a second null eigenvalue if the PHE has a series-flow arrangement with a number of channels multiple of four. In such cases, Eq. (A.4) must be used instead of Eq. (A.3).

$$\underline{\theta}(\eta) = \sum_{j=1}^{N_C-2} c_j \underline{Z_j} \exp(\lambda_j \eta) + c_{N_C-1} \underline{Z_{N_C-1}} \eta + c_{N_C} \underline{Z_{N_C}} \tag{A.4}$$

Appendix B. Detailing of steps 6, 9 and 10 of the assembling algorithm

In step 6 of the assembling algorithm, the channel flow direction parameters s_i ($i = 1, \ldots, N_C$) are determined. A procedure for the determination of this variable is presented as follows:

For $p = 1$ to P^{I} $\{^1$
For $n = 1$ to N^{I} $\{^2$
$i = 2(p-1)N^{\mathrm{I}} + 2n - 1$
$s_i = (-1)^{p+1}$ $\}^2$ $\}^1$
For $p = 1$ to P^{II} $\{^1$
For $n = 1$ to N^{II} $\{^2$
$i = 2(p-1)N^{\mathrm{II}} + 2n$
If $\phi = 1$: $s_i = (-1)^{p+1}$
If $\phi = 2$: $s_i = (-1)^{p}$
If $\phi = 3$: $s_i = (-1)^{P^{\mathrm{II}}+p}$
If $\phi = 4$: $s_i = (-1)^{P^{\mathrm{II}}+p+1}$ $\}^2$ $\}^1$

Note that $\{^1\}^1$ and $\{^2\}^2$ indicate distinct loops. This procedure to determine s_i can be easily implemented in usual programming languages.

The thermal boundary conditions for the system of equations (see Table 3) are built in steps 9 and 10 of the algorithm, respectively, for sides I and II of the PHE. Since the fluid path inside the exchanger needs to be followed in order to determine the connections among channels and passes, obtaining the boundary conditions

Table 6
Detailing of step 9 of the assembling algorithm

Boundary conditions for side I

Fluid inlet

For $n = 1$ to N^{I} $\{^1$
$\theta_{2n-1}(\eta = 0) = \theta_{\mathrm{in}}^{\mathrm{I}}$ $\}^1$

Fluid outlet

$$\theta_{\mathrm{out}}^{\mathrm{I}} = \frac{1}{N^{\mathrm{I}}}\sum_{i=1}^{N^{\mathrm{I}}}\theta_{2(P^{\mathrm{I}}-1)N^{\mathrm{I}}+2i-1}\left(\eta = \frac{(-1)^{P^{\mathrm{I}}+1}+1}{2}\right)$$

Change of pass

For $p = 2$ to P^{I} $\{^1$
For $n = 1$ to N^{I} $\{^2$

$$\theta_{2(p-1)N^{\mathrm{I}}+2n-1}\left(\eta = \frac{(-1)^{p}+1}{2}\right) = \frac{1}{N^{\mathrm{I}}}\sum_{i=1}^{N^{\mathrm{I}}}\theta_{2(p-2)N^{\mathrm{I}}+2i-1}\left(\eta = \frac{(-1)^{p}+1}{2}\right) \quad \}^2 \quad \}^1$$

Table 7
Detailing of step 10 of the assembling algorithm

Boundary conditions for side II when $\phi = 1$

Fluid inlet

For $n = 1$ to N^{II} $\{^1$
$\theta_{2n}(\eta = 0) = \theta_{\mathrm{in}}^{\mathrm{II}}$ $\}^1$

Fluid outlet

$$\theta_{\mathrm{out}}^{\mathrm{II}} = \frac{1}{N^{\mathrm{II}}}\sum_{i=1}^{N^{\mathrm{II}}}\theta_{2(P^{\mathrm{II}}-1)N^{\mathrm{II}}+2i}\left(\eta = \frac{(-1)^{P^{\mathrm{II}}+1}+1}{2}\right)$$

Change of pass

For $p = 2$ to P^{II} $\{^1$
For $n = 1$ to N^{II} $\{^2$

$$\theta_{2(p-1)N^{\mathrm{II}}+2n}\left(\eta = \frac{(-1)^{p}+1}{2}\right) = \frac{1}{N^{\mathrm{II}}}\sum_{i=1}^{N^{\mathrm{II}}}\theta_{2(p-2)N^{\mathrm{II}}+2i}\left(\eta = \frac{(-1)^{p}+1}{2}\right) \quad \}^2 \quad \}^1$$

Boundary conditions for side II when $\phi = 2$

Fluid inlet

For $n = 1$ to N^{II} $\{^1$
$\theta_{2n}(\eta = 1) = \theta_{\mathrm{in}}^{\mathrm{II}}$ $\}^1$

Fluid outlet

$$\theta_{\mathrm{out}}^{\mathrm{II}} = \frac{1}{N^{\mathrm{II}}}\sum_{i=1}^{N^{\mathrm{II}}}\theta_{2(P^{\mathrm{II}}-1)N^{\mathrm{II}}+2i}\left(\eta = \frac{(-1)^{P^{\mathrm{II}}}+1}{2}\right)$$

Change of pass

For $p = 2$ to P^{II} $\{^1$
For $n = 1$ to N^{II} $\{^2$

$$\theta_{2(p-1)N^{\mathrm{II}}+2n}\left(\eta = \frac{(-1)^{p+1}+1}{2}\right) = \frac{1}{N^{\mathrm{II}}}\sum_{i=1}^{N^{\mathrm{II}}}\theta_{2(p-2)N^{\mathrm{II}}+2i}\left(\eta = \frac{(-1)^{p+1}+1}{2}\right) \quad \}^2 \quad \}^1$$

Boundary conditions for side II when $\phi = 3$

Fluid inlet

For $n = 1$ to N^{II} $\{^1$
$\theta_{2(P^{\mathrm{II}}-1)N^{\mathrm{II}}+2n}(\eta = 0) = \theta_{\mathrm{in}}^{\mathrm{II}}$ $\}^1$

Fluid outlet

$$\theta_{\mathrm{out}}^{\mathrm{II}} = \frac{1}{N^{\mathrm{II}}}\sum_{i=1}^{N^{\mathrm{II}}}\theta_{2i}\left(\eta = \frac{(-1)^{P^{\mathrm{II}}+1}+1}{2}\right)$$

Change of pass

For $p = 2$ to P^{II} $\{^1$
For $n = 1$ to N^{II} $\{^2$

$$\theta_{2(p-2)N^{\mathrm{II}}+2n}\left(\eta = \frac{(-1)^{P^{\mathrm{II}}+p}+1}{2}\right) = \frac{1}{N^{\mathrm{II}}}\sum_{i=1}^{N^{\mathrm{II}}}\theta_{2(p-1)N^{\mathrm{II}}+2i}\left(\eta = \frac{(-1)^{P^{\mathrm{II}}+p}+1}{2}\right) \quad \}^2 \quad \}^1$$

Boundary conditions for Side II when $\phi = 4$

Fluid inlet

For $n = 1$ to N^{II} $\{^1$
$\theta_{2(P^{\mathrm{II}}-1)N^{\mathrm{II}}+2n}(\eta = 1) = \theta_{\mathrm{in}}^{\mathrm{II}}$ $\}^1$

Fluid outlet

$$\theta_{\mathrm{out}}^{\mathrm{II}} = \frac{1}{N^{\mathrm{II}}}\sum_{i=1}^{N^{\mathrm{II}}}\theta_{2i}\left(\eta = \frac{(-1)^{P^{\mathrm{II}}}+1}{2}\right)$$

Change of pass

For $p = 2$ to P^{II} $\{^1$
For $n = 1$ to N^{II} $\{^2$

$$\theta_{2(p-2)N^{\mathrm{II}}+2n}\left(\eta = \frac{(-1)^{P^{\mathrm{II}}+p+1}+1}{2}\right) = \frac{1}{N^{\mathrm{II}}}\sum_{i=1}^{N^{\mathrm{II}}}\theta_{2(p-1)N^{\mathrm{II}}+2i}\left(\eta = \frac{(-1)^{P^{\mathrm{II}}+p+1}+1}{2}\right) \quad \}^2 \quad \}^1$$

of exchangers with large number of plates is not a simple task. An automatic procedure to generate the set of boundary conditions equations is presented in Tables 6 and 7 for sides I and II of the exchanger, respectively.

References

[1] A.A. McKillop, W.L. Dunkley, Plate heat exchangers: heat transfer, Ind. Eng. Chem. 52 (9) (1960) 740–744.

[2] M. Masubuchi, A. Ito, Dynamic analysis of a plate heat exchanger system, Bull. JSME 20 (142) (1977) 434–441.

[3] A. Settari, J.E.S. Venart, Approximate method for the solution to the equations for parallel and mixed-flow multichannel heat exchangers, Int. J. Heat Mass Transfer 15 (1972) 819–829.

[4] T. Zaleski, K. Klepacka, Approximate methods of solving equations for plate heat-exchangers, Int. J. Heat Mass Transfer 35 (1992) 1125–1130.

[5] S.G. Kandlikar, R.K. Shah, Asymptotic effectiveness-NTU formulas for multipass plate heat exchangers, J. Heat Transfer 111 (1989) 314–321.

[6] T. Zaleski, A.B. Jarzebski, Remarks on some properties of equation of heat-transfer in multichannel exchangers, Int. J. Heat Mass Transfer 16 (8) (1973) 1527–1530.

[7] T. Zaleski, A general mathematical-model of parallel-flow, multichannel heat-exchangers and analysis of its properties, Chem. Eng. Sci. 39 (7/8) (1984) 1251–1260.

[8] S.G. Kandlikar, R.K. Shah, Multipass plate heat exchangers-effectiveness-NTU results and guidelines for selecting pass arrangements, J. Heat Transfer 111 (1989) 300–313.

[9] M.C. Georgiadis, S. Macchietto, Dynamic modeling and simulation of plate heat exchangers under milk fouling, Chem. Eng. Sci. 55 (2000) 1605–1619.

[10] T. Zaleski, K. Klepacka, Plate heat-exchangers-method of calculation, charts and guidelines for selecting plate heat-exchangers configurations, Chem. Eng. Process. 31 (1) (1992) 45–56.

[11] Process Systems Enterprise Ltd., gPROMS Introductory User Guide, Release 2.0, London, 2001.

[12] J. Taborek, Shell-and-tube heat exchangers: single-phase flow, in: G.F. Hewitt (Ed.), Handbook of Heat Exchanger Design, Begell House, New York, 1992, p. s.3.3.

[13] S. Kakaç, H. Liu, Heat Exchangers: Selection, Rating and Thermal Design, CRC Press, New York, 1998, pp. 232–354.

[14] R.K. Shah, W.W. Focke, Plate heat exchangers and their design theory, in: R.K. Shah, E.C. Subbarao, R.A. Mashelkar (Eds.), Heat Transfer Equipment Design, Hemisphere, New York, 1988, pp. 227–254.

[15] R.A. Buonopane, R.A. Troupe, J.C. Morgan, Heat transfer design method for plate heat exchangers, Chem. Eng. Progress 57 (7) (1963) 57–61.

[16] J.M. Pinto, J.A.W. Gut, A screening method for the optimal selection of plate heat exchanger configurations, Brazil. J. Chem. Eng. 19 (4) (2002) 433–439.

[17] A. Pignotti, P.I. Tamborenea, Thermal effectiveness of multipass plate exchangers, Int. J. Heat Mass Transfer 31 (10) (1988) 1983–1991.

[18] A. Pignotti, Flow reversibility of heat exchangers, J. Heat Transfer 106 (1984) 361–368.

[19] M.K. Bassiouny, H. Martin, Flow distribution and pressure drop in plate heat exchangers—I, U-type arrangement, Chem. Eng. Sci. 39 (4) (1984) 693–700.

[20] E.A.D. Saunders, Heat Exchangers: Selection, Design and Construction, Longman S. & T, New York, 1988, s. 4, 16, 17.

[21] M.A. Mehrabian, R. Poulter, G.L. Quarini, Hydrodynamic and thermal characteristics of corrugated channels: experimental approach, Experiment. Heat Transfer 13 (3) (2000) 223–235.

[22] F. Delplace, J.C. Leuliet, Generalized Reynolds number for the flow of power law fluids in cylindrical ducts of arbitrary cross-section, Chem. Eng. J. 56 (1995) 33–37.

[23] J. Marriott, Where and how to use plate heat exchangers, Chem. Eng. 5 (1971) 127–134.

[24] P. Honig, Principios de la Tecnologia Azucarera, Continental, Mexico, vol. 1, 1969.

[25] O. Lyle, Technology for Sugar Refinery Workers, third ed., Chapman & Hall, London, 1970.

[26] K. Schwier, Properties of liquid water, in: G.F. Hewitt (Ed.), Handbook of Heat Exchanger Design, Begell House, New York, 1992, p. s.5.5.3.

[27] C.O. Bennett, J.E. Myers, Momentum, Heat and Mass Transfer, third ed., McGraw-Hill, London, 1982.

[28] R.H. Perry, D.W. Green, J.O. Maloney, Perry's Chemical Engineers' Handbook, seventh ed., McGraw-Hill, New York, 1997.

[29] M.K. Bassiouny, H. Martin, Temperature distribution in a four channel plate heat exchanger, Heat Transfer Eng. 6 (2) (1985) 58–72.

[30] A. Varma, M. Morbidelli, Mathematical Methods in Chemical Engineering, Oxford University Press, New York, 1997.